Journal of Hazardous Materials 192 (2011) 1548–1554

Contents lists available at ScienceDirect

Journal of Hazardous Materials

journal homepage: www.elsevier.com/locate/jhazmat

Synthesis of mesoporous β-Ga_2O_3 nanorods using PEG as template: Preparation, characterization and photocatalytic properties

Weirong Zhao[a,b,*], Yong Yang[a], Rui Hao[a], Feifei Liu[a], Yan Wang[a], Min Tan[a], Jing Tang[a], Daqing Ren[a], Dongye Zhao[b]

[a] Department of Environmental Engineering, Zhejiang University, Hangzhou 310058, China
[b] Environmental Engineering Program, Department of Civil Engineering, Auburn University, Auburn, AL 36849, USA

ARTICLE INFO

Article history:
Received 25 March 2011
Received in revised form 15 June 2011
Accepted 27 June 2011
Available online 1 July 2011

Keywords:
β-Ga_2O_3
Photocatalyst
Toluene
Toxicity
Indoor air

ABSTRACT

Mesoporous wide bandgap semiconductors offer high photocatalytic oxidation and mineralization activities. In this study, mesoporous β-Ga_2O_3 diamond nanorods with 200–300 nm in diameter and 1.0–1.2 μm in length were synthesized via a urea-based hydrothermal method using polyethylene glycol (PEG) as template agent. The UV photocatalytic oxidation activity of β-Ga_2O_3 for gaseous toluene was evaluated, and 7 kinds of intermediates were monitored online by a proton transfer reaction mass spectrometry. Photoluminescence spectra manifested that the dosage and molecular weight of PEG are crucial for formation of vacancies and photocatalytic oxidation activities. A PEG-assisted hydrothermal formation mechanism of mesoporous β-Ga_2O_3 diamond nanorods was proposed. Based on the health risk influence index (η) of the intermediates, the calculated health risks revealed that the β-Ga_2O_3 nanorods with a η value of 9.6 are much safer than TiO_2 (η = 17.6).

1. Introduction

Mesoporous (2–50 nm) structures can serve as robust templates for incorporation of quantum-confined inorganic semiconductor sensitizers [1], and have been widely used in the area of molecular separation, sorption or as catalysts and catalyst supports [2]. Because of their uniquely larger specific surface area, continuous pore channels, and multiple scattering structures, mesoporous materials have been widely used as photocatalysts of high light harvesting and fast mass transfer rate [3].

Wide bandgap metal oxide photocatalysts such as β-Ga_2O_3 (E_g = 4.9 eV) [4] and $ZnGa_2O_4$ (E_g = 4.4–5.0 eV) [5] bear dispersive conduction band, which can promote the mobility of the photogenerated electrons and enhance the charge separation [6]. As a result, these photocatalysts show exceptional performance in photocatalytic oxidation of volatile organic compounds (VOCs) into harmless compounds such as carbon dioxide and water. Recently, 1-dimensional β-Ga_2O_3 such as nanowires and nanorods has attracted increasing attention for its unique nanostructure and photocatalytic properties. Many synthesis methods have been proposed, including microwave plasma [7], arc discharge method [8], thermal evaporation [9], carbothermal reduction [10], hydrothermal method [11], and sol–gel method [4]. In particular, the hydrothermal method has elicited great interest in preparing uniform and stable catalysts because it is a simple wet chemical process and can be carried out at low temperatures [12].

High surface area mesoporous nano- or micro-structures are believed to offer much improved photocatalytic activity than conventional low-surface area counterparts, especially in multiphase photocatalytic systems [13]. In such systems, the reaction rate of gas–solid heterogeneous photocatalysis is often limited by mass-transfer processes on the catalyst surface [14]. For instance, mesoporous TiO_2 [15] and zeolite-supported TiO_2 with a larger surface area showed efficient photocatalytic activity, especially for gas phase reactions [16]. Therefore, developing porous β-Ga_2O_3 with a larger surface area is of great scientific and practical significance.

Surfactant templating has provided a breakthrough methodology for preparation of a number of mesoporous materials with a variety of mesophases, 2- or 3-dimensional pore networks and diverse tunable properties [17]. Of various surfactants used, polyethyl glycol (PEG) is an important templating reagent for synthesizing mesoporous nanomaterials [18].

The overall goal of this study was to prepare and characterize a class of PEG-modified β-Ga_2O_3 mesoporous nanorods by a modified hydrothermal method toward the photocatalytic oxidation of VOCs. The specific objectives were to: (1) determine the effects of molecular weight and the content of PEG on the BET area

* Corresponding author at: Department of Environmental Engineering, Zhejiang University, Zheda Road 38, Hangzhou 310058, China. Tel.: +86 571 8898 2032; fax: +86 571 8898 2032.
E-mail address: weirong@mail.hz.zj.cn (W. Zhao).

0304-3894/$ – see front matter © 2011 Elsevier B.V. All rights reserved.
doi:10.1016/j.jhazmat.2011.06.073

and photoluminescence (PL) toward better understanding of the crystalline growth process; (2) assess the environmental friendliness of the β-Ga_2O_3 facilitated photocatalytic oxidation process based on recommended exposure limit (REL) and the health risk influence index (η) via evaluating the photocatalytic degradation of toluene (a prototype VOC) and identifying the photocatalytic oxidation intermediates using a proton transfer reaction mass spectrometry (PTR-MS).

2. Experimental

2.1. Materials and synthesis

All chemicals were used as purchased without further purification in this study. The nanoscale β-Ga_2O_3 rods were prepared via the PEG assisted hydrothermal method. In a typical synthesis process, 1.6 g $Ga(NO_3)_3{\cdot}9H_2O$ (AR, Longjin Material, China), 2.64 g urea (AR, Sinopharm Chemical Reagent, China), and 20 mL PEG (AR, Gaonan Chemical Reagent, China) were dissolved into 70 mL of deionized water and then stirred vigorously for 2 h at 25 ± 1 °C. The solution was then transferred into a Teflon-lined stainless steel autoclave (100 mL in capacity) and hydrothermally reacted at 140 °C for 6 h. After the reaction, the white precipitates were filtrated and washed with deionized water and then absolute ethanol for 3–5 times in order to remove any possible impurities. The material was then calcined at 800 °C for 2 h in a muffle furnace to acquire the desired nanostructured of β-Ga_2O_3 nanorods. Commercial P25 TiO_2 (Degussa, Germany) was used as the control catalyst.

2.2. Characterizations and measurements

The morphologies of the samples were investigated by a scanning electron microscopy (SEM) (Model S-570, Hitachi, Japan), the nanostructure and crystalline of samples were examined by a transmission electron microscopy (TEM), a high-resolution transmission electron microscopy (HRTEM), and a selected area electron diffraction (SAED) (JEM-2010, Jeol, Japan) at an accelerating voltage of 200 kV. The photoluminescence (PL) spectra were measured at 25 ± 1 °C with a fluorospectrophotometer (Fluorolog-3-Tau, France) using a Xe lamp as the excitation source.

2.3. Online detection of photocatalytic oxidation intermediates

The photocatalytic oxidation intermediates were monitored in a continuous flow-through reactor (30 mL) made of Teflon and quartz glass (transmittance wavelength > 250 nm) irradiated with three 4 W monochrome UV-lamps (G4T5L, Yaguang, China) over quartz glass at 25 ± 1 °C. The intermediates were analyzed online using PTR-MS (Ionicon Analytik, Austria). See text S1 of Supplementary Information for further details.

2.4. Photocatalytic activity tests

Photocatalytic oxidation of toluene, a typical indoor air pollutant, was chosen as the probe reaction to characterize the activity of the as-prepared samples [19]. Another reactor was also equipped with four 2 W monochrome UV-lamps (G2T5L, Yaguang, China) with a light emission wavelength of 254 nm. The initial concentration of toluene was controlled at 160 or 200 ppm taking into account the adsorption equilibrium of toluene with the catalyst in the reactor, and the concentration of toluene was analyzed by a GC-FID (9790, Fuli, China). There was no degradation observed in the absence of the catalyst.

3. Results and discussion

3.1. Photocatalyst characterizations

The diffraction peaks in the XRD patterns (Fig. S1a and b) can be indexed to the precursor GaOOH and monoclinic β-Ga_2O_3 according to JCPDS: 06-0180 and JCPDS: 41-1103, respectively.

Fig. 1 shows the morphology and structure of the as-prepared β-Ga_2O_3 with SEM and TEM (HRTEM). Fig. 1a shows the SEM image of the β-Ga_2O_3 nanorods which exhibits a diamond crossing-section with two 60° and two 120° angles. Also, there are many nanoscale holes/cavities on the surface of the samples, which is similar to the quadrilateral β-Ga_2O_3 prisms reported by Zhang et al. [11]. It is also evident that the β-Ga_2O_3 nanorod grew along the [1 1 1] direction. Fig. 1b–d shows the TEM images of the β-Ga_2O_3 nanorods. The β-Ga_2O_3 nanorods have an appearance of 200–300 nm of each side and 1.0–1.2 μm in length with dense nanoholes whose average diameter is ca. 20 nm. The HRTEM images in Fig. 1e and f suggest the clear (1 1 1), (2 0 1), and (4 0 0) lattice fringes with the interplanar spacing of 0.25, 0.37, and 0.28 nm, respectively. The SAED pattern in Fig. 1e (inset) shows intense electron diffraction rings, consistent with the partial crystallinity of the β-Ga_2O_3 walls as reported by West et al. [20]. The EDX spectrum (Fig. S2) indicates the peaks of Ga, O, and N. The atomic ratio of gallium to oxygen is about 2: 2.87. Compared to the stoichiometric of Ga_2O_3, there are 4.3% oxygen vacancies in the β-Ga_2O_3 nanorods [21]. A small amount of N impurity comes from the urea, which is doped during sample calcining at 800 °C. Although C dopant is expected to result from urea and PEG during the hydrothermal process, it is not detected possibly due to its relatively high detection limit (0.5%).

The surface area of the β-Ga_2O_3 is determined to be 28.98 m^2/g, and the pore size of the sample predominantly falls in the mesoporous range from 10 to 50 nm (Fig. S3).

The direct bandgap of the β-Ga_2O_3 nanorods (Fig. S4) is about 4.4 eV, which is a little bit narrower than 4.9 eV reported by Hou et al. [4]. N doping can form new states just above the valence band for substitutional or interstitial nitrogen, which could narrow down the bandgap of β-Ga_2O_3 by mixing the N 2p with O 2p states, and this is similar to the findings with N doped TiO_2 in our previous studies [19,22].

3.2. Intermediates of photocatalytic oxidation process

Fig. 2 shows the distribution of intermediates during TiO_2 and β-Ga_2O_3 facilitated photocatalytic oxidation of toluene and the health risk index (HRI) values. In order to evaluate adverse negative effects of the intermediates, HRI for the intermediates was employed on the model introduced by Mo et al. [23]. A health risk influence index η can be deduced as follows:

$$\eta = \frac{\sum HRI_{i,outlet}}{\sum HRI_{i,inlet}} = \frac{\sum (C_i/REL_i)_{outlet}}{\sum (C_i/REL_i)_{inlet}} \quad (1)$$

where $\Sigma HRI_{i,outlet}$ and $\Sigma HRI_{i,inlet}$ are the sum of HRI values of the gaseous intermediates in the outlet and inlet gases, respectively. The recommended exposure limit (REL) of compound i was obtained from the toxicity database of Integrated Risk Information System (IRIS) [24]. The values of REL of different intermediates were listed in Table S1. A value of $\eta > 1$, <1, and =1 indicates that the health risk of the intermediates formed in photocatalytic oxidation is higher, lower, and equal to their parent compound, respectively.

Fig. 2a shows the distribution of intermediates for both TiO_2 and β-Ga_2O_3 (optimized with 20 mL PEG200) catalysts. The intermediates include formaldehyde, methanol, acetaldehyde, 1,3-butadiene, acraldehyde, acetone, and acetic acid. These intermediates are generated in the photocatalytic oxidation process and emitted

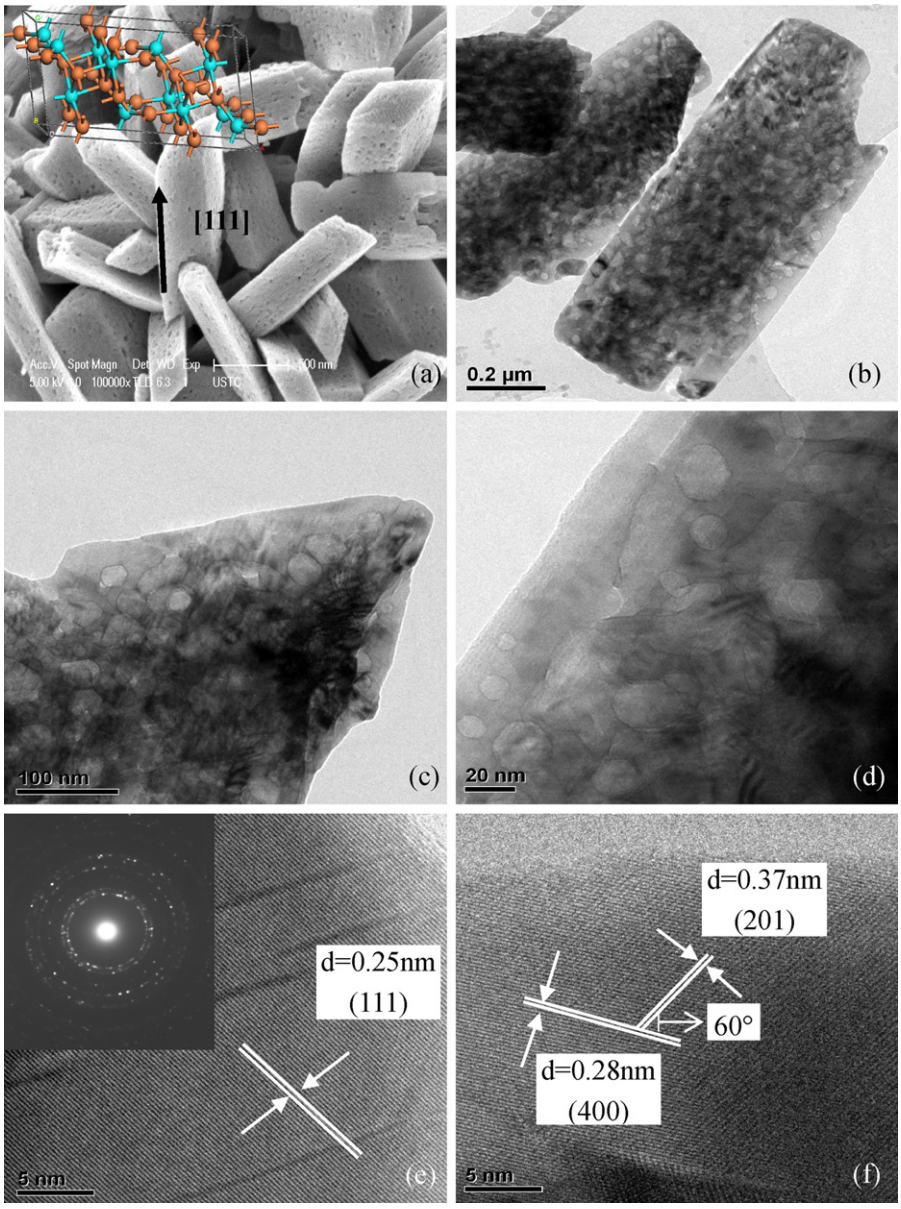

Fig. 1. Characterization of β-Ga_2O_3 nanorods prepared with 20 mL dosage of PEG200. (a) SEM image and 3D model (inset) of the β-Ga_2O_3 nanorods, (b–d) close up TEM images, and (e and f) HRTEM images and electron diffraction rings (inset).

to the gaseous phase. Formaldehyde and acetaldehyde are considered more toxic than toluene [24]. It is evident that β-Ga_2O_3 produced much less percentage of toxic intermediates such as acetaldehyde and formaldehyde than the TiO_2 counterpart. In fact, β-Ga_2O_3 resulted in more percentage of benign intermediates such as methanol, 1,3-butadiene, and acetic acid than TiO_2. Methanol is the predominant intermediate for β-Ga_2O_3, accounting for 36.1% of the total intermediates. In contrast, acetaldehyde accounts for 60.0% of the intermediates for TiO_2. Evidently, β-Ga_2O_3 can lead to more reduced production of acetaldehyde and formaldehyde in the photocatalytic oxidation process than TiO_2. Although β-Ga_2O_3 modestly increases the percentage concentration of acraldehyde and 1,3-butadiene, this drawback is outweighed by the conversion of much greater fractions of innocuous acetic acid and alcohol.

Fig. 2b shows the HRI and η values increased from 174 and 9.6 for β-Ga_2O_3 to 290 and 17.7 for TiO_2, respectively. Evidently, the wide bandgap β-Ga_2O_3 can serve as a cleaner photocatalyst than TiO_2 based on the toxicity analysis of the intermediates. This difference can be attributed to the difference in the band structures between β-Ga_2O_3 with TiO_2.

Typically, photocatalytic processes are controlled by two pathways: hydroxyl radical (•OH) oxidation and photoinduced holes oxidation [25,26]. The •OH produced from water is controlled by the water molecular on the surface of the photocatalysts or the RH of gas, while photoinduced holes oxidation properties are strongly dependent on the structural and electronic properties of the photocatalysts. The wider bandgap of β-Ga_2O_3 endows the photogenerated holes with stronger oxidation potentials [27,28]. The electron holes can either react with surface adsorbed H_2O to give more •OH or directly transfer electrons from the target pollutants to the holes, leading to highly oxidized compounds such as organic acids or alcohol which are less toxic.

3.3. Influence of molecular weight of PEG

Fig. 3a shows the PL spectra measured under vacuum condition at 300 K for the β-Ga_2O_3 nanorods synthesized following the

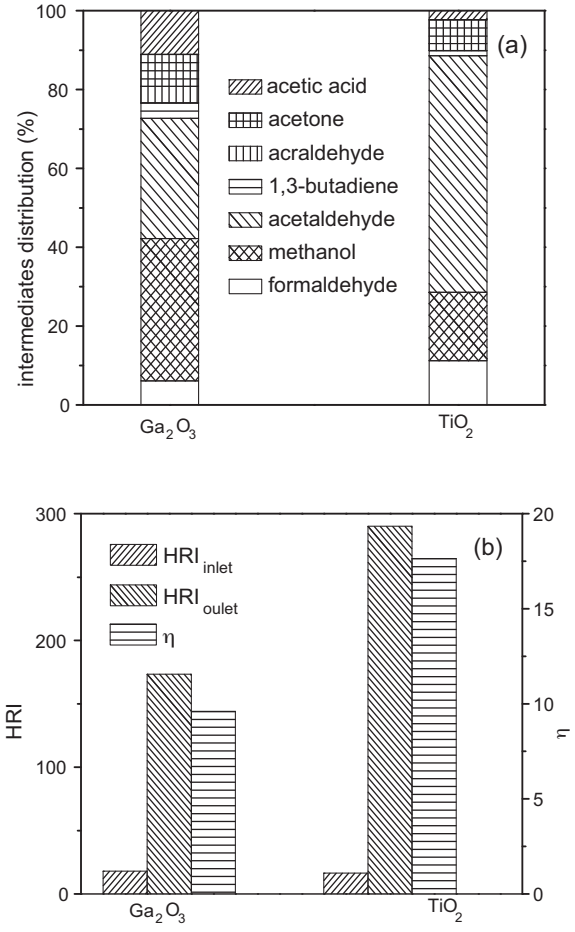

Fig. 2. Photocatalytic oxidation of toluene with β-Ga_2O_3 or TiO_2. (a) Intermediates distribution, and (b) HRI and η values. Experimental condition: RH = 45% and $C_{toluene}$ = 200 ppb.

same hydrothermal method but with PEGs of various M.W. The samples prepared with PEG of different M.W. exhibit an obvious PL signal with a similar curve shape, demonstrating that the PEGs do not result in a new PL phenomenon. All of the PL spectra are strong at the wavelength ranging from 300 to 800 nm, with three obvious PL peaks at about 455, 690, and 710 nm, respectively. The spectra are deconvoluted with four Gaussian curves with peaks at 450, 520, 695, and 720 nm. A strong blue PL emission is centered at ca. 450 nm. The blue luminescence in β-Ga_2O_3 can be attributed to vacancies such as gallium vacancies (V_{Ga}), oxygen vacancies (V_O), and gallium-oxygen vacancy pairs (V_O, V_{Ga}) [29]. The EDX spectrum of β-Ga_2O_3 in Fig. S2 proves that there are oxygen defects. Therefore, the blue luminescence should be attributed to the oxygen vacancies V_O. The Gaussian curves with peaks at 520 nm should be gallium-oxygen vacancy pairs (V_O, V_{Ga}) [30,31]. Another two peaks centered at 695 and 720 nm should be attributed to carbon and nitrogen dopants resulting from urea and PEG in the hydrothermal process, respectively. The carbon and nitrogen doping generates deep acceptor levels in the bandgap of β-Ga_2O_3, and the position of the doping-induced sub-bands is around at the center of the bandgap. The electron traps on a donor and the hole trapped on an acceptor will recombine radiatively, emitting photons with wavelength around 695 and 720 nm. It was reported that nitrogen dopants acted as electron acceptors in β-Ga_2O_3 inducing holes traps and it recombined with electrons trapped at oxygen vacancy donors, generating red-light emission [32]. The decrease in the representative photoluminescence intensity at 450 nm indicates that the intersystem crossing of excitons is hindered as a consequence of weakening spin orbital coupling as the M.W. of PEG increases [33]. As a result, fewer electrons in the excited singlet jump into the triplet state by the intersystem crossing, which leads to less efficient photoluminescence. The PEG with higher M.W. should have longer molecular chain, which makes the molecular itself coiled or spiraled with other PEG molecules via hydrogen bonding in the solution and leads to lessened effective number of PEG and surface area that could interact with GaOOH. Consequently, fewer oxygen vacancies would be produced, and thus the PL intensity decreases with increasing M.W. of PEG template. However, the PL intensity is not only related with the concentration of vacancies, but also the distribution of vacancies. The uneven distribution of vacancies may cause uneven absorption of photons, resulting in decreased emission of luminescence.

Notably, as can be seen from Fig. S5, the samples prepared by different M.W. of PEG are all diamond rodlike, indicating that there is no obvious effect on the morphology of samples. The activity of β-Ga_2O_3 synthesized by PEG200 (PEG of M.W. = 200) shows the biggest BET surface area (29.0 m^2/g) and the strongest catalytic activity. The photocatalytic activity decreases with increasing M.W. of PEG (see Fig. S6 and the details).

3.4. Influence of PEG dosage

Fig. S5 shows the dosage of PEG200 influence on the morphology of samples unnoticeably. Table S2 gives the results of the BET

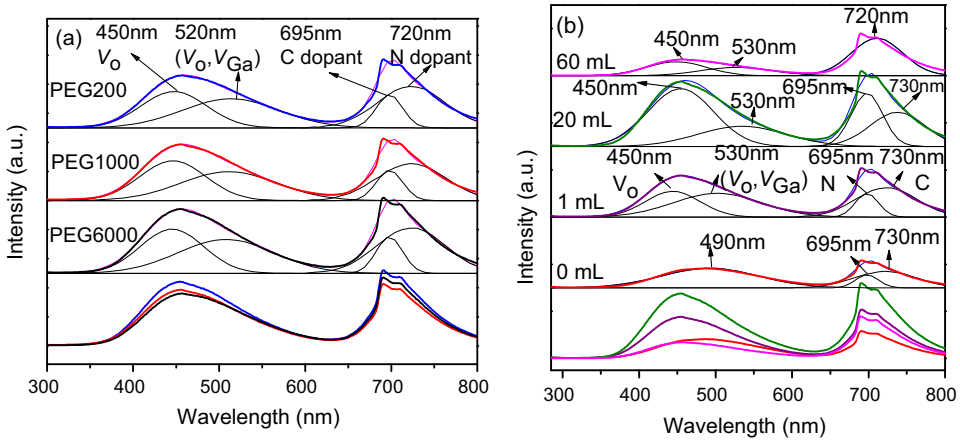

Fig. 3. PL spectra excited at wavelength of 260 nm and the distribution of four kinds spectra of vacancies: (a) influence of molecular weights of PEG by the addition of 1 mL, and (b) influence of PEG200 dosage.

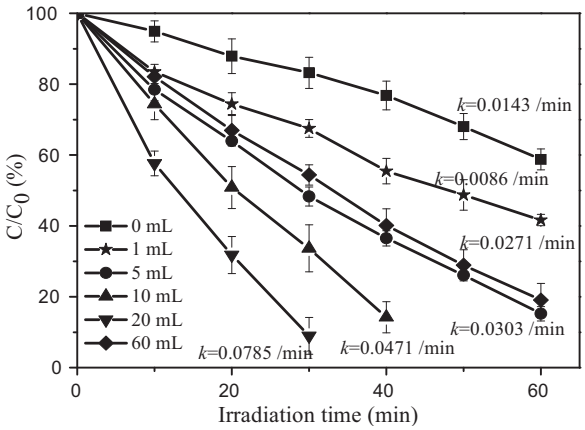

Fig. 4. The photocatalytic oxidation rates of gaseous toluene. Experimental condition: RH = 45%, and $C_{toluene}$ = 200 ppm.

surface area of β-Ga_2O_3 nanorods prepared at various dosage of PEG200. The crystallite size continuously decreases and the surface area increases to the optimum value of 29.0 m^2/g when the addition of PEG200 is increased to 20 mL. However, further increase of PEG to 60 mL sharply decreases the BET surface area to 10.6 m^2/g, which can be attributed to the unstable pore structure induced by the burnout of PEG200 at particularly high concentrations, where most of the mesoporous framework could be easily damaged upon thermal treatment, resulting in considerable aggregation and structure defects of crystals and a sharp decrease of surface area. Therefore, the dosage of PEG is also an important factor to control the crystal size and nanostructure of β-Ga_2O_3 nanorods.

Fig. 3b shows the PL spectra of β-Ga_2O_3 nanorods synthesized with different dosage of PEG200 using the excitation light of 260 nm at 300 K. It shows that the PEG dosage has a great effect on the PL intensity of the β-Ga_2O_3 nanorods. The PL intensity increases with increasing PEG content and reaches the highest degree at PEG dosage of 20 mL. When the PEG dosage is higher than 60 mL, the PL intensity drops sharply, this is in accord with the XRD findings in Fig. S7. The spectra are deconvoluted with three or four Gaussian curves. Fig. 3b shows that there are three Gaussian curves with peaks at 490, 695, and 730 nm of PL spectra for the samples synthesized without PEG200, which is different from those for samples synthesized with 1 and 20 mL PEG200 at 450, 510 (530), 695, and 730 nm. For the sample without PEG, the weak peak at 490 nm should be attributed to gallium-oxygen vacancy pairs (V_O, V_{Ga}), as this sample has a low concentration of oxygen vacancy. The two Gaussian peaks at 695 and 730 nm in the PL spectra of the sample synthesized without PEG200 indicate that urea can provide N and C dopants. With the addition of PEG, the concentration of C dopant in the samples increases, whereas the concentration of N dopant remains constant. When the high dosage of PEG as 60 mL of PEG200 was added, it results in formation of micelles (the critical micelle concentration ca. 20 mL), which in turn lead to uneven distribution of the vacancies, with weak vacancies being covered. Consequently, only one Gaussian peak at 720 nm is evident. The uneven distribution of vacancies can vary the Gaussian peaks which are somewhat different showed in Fig. 3b, and it makes some Gaussian curves disappear or peaks shift. Therefore, the separation abilities of photo-induced charges of β-Ga_2O_3 can be improved by modifying the content of PEG because the oxygen vacancies can easily capture or bind photo-induced electrons.

Fig. 4 compares the photocatalytic activities of β-Ga_2O_3 synthesized with different dosage of PEG200 at RH of 45% and initial toluene of 200 ppm. At the PEG200 dosage of 20 mL, the activity of β-Ga_2O_3 is the highest (k = 0.0785/min) which is in accord with the results of PL spectra at 450 nm shown in Fig. 3b. However, the PL intensity of the sample with 60 mL of PEG200 is lower than that without PEG200, but the photocatalytic activity of β-Ga_2O_3 synthesized with 60 mL PEG200 (k = 0.0271/min) is higher than that without PEG200 (k = 0.0086/min). Apparently, when the concentration of oxygen vacancies is lower, the photocatalytic activity correlates well with the PL intensity and oxygen vacancies. However, if the concentration of oxygen vacancies is higher, oxygen vacancies become combination centers that decrease the photocatalytic activity.

3.5. Formation mechanism of mesoporous β-Ga_2O_3

According to the results above, the formation mechanism of mesoporous β-Ga_2O_3 nanorods is proposed in Fig. 5. First, GaOOH nanoparticles are produced when urea is slowly hydrolyzed into the

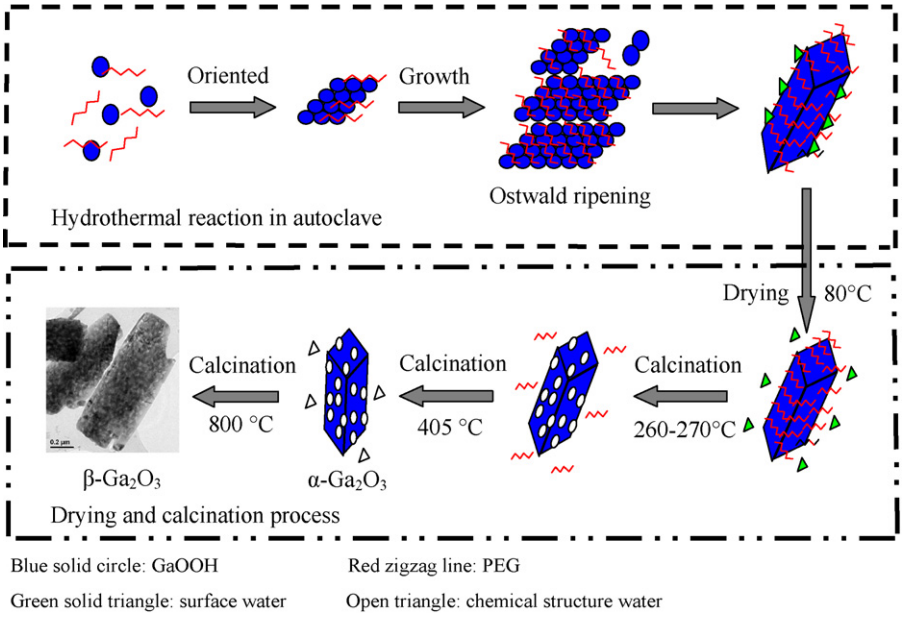

Fig. 5. A proposed schematic processes for the fabrication of mesoporous β-Ga_2O_3 nanorods.

weak base NH_4OH and CO_2 gas (Fig. S8). The hydrophilic groups in the polymeric chain of PEG are adsorbed on the surface of GaOOH nanoparticles to minimize their surface energy, preventing rapid aggregation of the particles. Consequently, GaOOH nanorods are formed via oriented attachment [34]. The SEM image (Fig. S5a) shows that the β-Ga_2O_3 particles can grow up into nonporous nanorods without PEG, and mixed with miscellaneous shapes. PEG plays an important role as a template in optimizing the growth orientation and the growth rate in the formation of the crystallites. Then, the crystallites grow further into diamond nanorods via Ostwald ripening [35]. As the diamond nanorods grow mature, some of the PEG and water molecules depart from the nanorods gradually. After drying at 80 °C, the water molecules absorbed on the surface of the products evaporate thoroughly, and later in the process of calcination, PEG molecules evaporate completely at 260–270 °C leading to formation of the mesoporous nanorods. Then, the calcination of the GaOOH nanorods results in α-Ga_2O_3 by dehydration at 405 °C, and then the perfect phase β-Ga_2O_3 at 800 °C. Here the high temperature can activate atoms in β-Ga_2O_3, the remaining PEG and urea molecules, so that N and C impurities with enough energy could enter into the β-Ga_2O_3 and replace the oxygen atoms.

4. Conclusion

(1) Mesoporous β-Ga_2O_3 diamond nanorods were synthesized via a hydrothermal method using PEG as template. The PEG with M.W. 200 and dosage of 20 mL as the optimal condition gives the largest BET surface area (29.0 m^2/g) and mean pore size of 30 nm. Oxygen vacancies (V_O), gallium-oxygen vacancy pairs (V_O, V_{Ga}), C and N dopants are the constituents of the PL peaks.
(2) Wide bandgap β-Ga_2O_3 shows greater photocatalytic performance and produces less toxic intermediates in the photocatalytic oxidation of toluene compared to the conventional catalyst TiO_2. The main intermediates include formaldehyde, alcohol, acetaldehyde, 1,3-butadiene, acraldehyde, acetone, and acetic acid. The percentage of more toxic intermediates, such as acetaldehyde and formaldehyde, is much lower with the new catalyst. The β-Ga_2O_3 photocatalytic oxidation process is much "greener" than the commercial TiO_2-mediated photocatalytic process.

Acknowledgments

This research was partially funded by the Zhejiang Provincial Natural Science Foundation of China (Grant No. Y5090149), the Chinese Key Technology Research and Development Program of the Eleventh Five-Year Plan (Grant No. 2006BAJ02A08), and the National Technology Research and Development Program ("863" Program) of China (Grant No. 2007AA061402).

Appendix A. Supplementary data

Supplementary data associated with this article can be found, in the online version, at doi:10.1016/j.jhazmat.2011.06.073.

References

[1] G.D. Chen, L. Jiang, L.Z. Wang, J.L. Zhang, Synthesis of mesoporous ZSM-5 by one-pot method in the presence of polyethylene glycol, Microporous Mesoporous Mater. 134 (2010) 189–194.
[2] J.G. Yu, G.H. Wang, B. Cheng, M.H. Zhou, Effects of hydrothermal temperature and time on the photocatalytic activity and microstructures of bimodal mesoporous TiO_2 powders, Appl. Catal. B: Environ. 69 (2007) 171–180.
[3] G.S. Li, J.C. Yu, J.A. Zhu, Y. Cao, Hierarchical mesoporous grape-like titania with superior recyclability and photoactivity, Microporous Mesoporous Mater. 106 (2007) 278–283.
[4] Y.D. Hou, W.C. Wang, L. Wu, Z.X. Ding, X.Z. Fu, Efficient decomposition of benzene over a beta-Ga_2O_3 photocatalyst under ambient conditions, Environ. Sci. Technol. 40 (2006) 5799–5803.
[5] X. Chen, H. Xue, Z.H. Li, L. Wu, X.X. Wang, X.Z. Fu, Ternary wide band gap p-block metal semiconductor $ZnGa_2O_4$ for photocatalytic benzene degradation, J. Phys. Chem. C 112 (2008) 20393–20397.
[6] H. Xue, Z. Li, L. Wu, Z. Ding, X. Wang, X. Fu, Nanocrystalline ternary wide band gap p-block metal semiconductor $Sr_2Sb_2O_7$: hydrothermal syntheses and photocatalytic benzene degradation, J. Phys. Chem. C 112 (2008) 5850–5855.
[7] S. Sharma, M.K. Sunkara, Direct synthesis of gallium oxide tubes, nanowires, and nanopaintbrushes, J. Am. Chem. Soc. 124 (2002) 12288–12293.
[8] Y.C. Choi, W.S. Kim, Y.S. Park, S.M. Lee, D.J. Bae, Y.H. Lee, G.S. Park, W.B. Choi, N.S. Lee, J.M. Kim, Catalytic growth of beta-Ga_2O_3 nanowires by arc discharge, Adv. Mater. 12 (2000) 746.
[9] B.Y. Geng, L.D. Zhang, G.W. Meng, T. Xie, X.S. Peng, Y. Lin, Large-scale synthesis and photoluminescence of single-crystalline beta-Ga_2O_3 nanobelts, J. Cryst. Growth 259 (2003) 291–295.
[10] X.C. Wu, W.H. Song, W.D. Huang, M.H. Pu, B. Zhao, Y.P. Sun, J.J. Du, Crystalline gallium oxide nanowires: intensive blue light emitters, Chem. Phys. Lett. 328 (2000) 5–9.
[11] J. Zhang, Z.G. Liu, C.K. Lin, J. Lin, A simple method to synthesize beta-Ga_2O_3 nanorods and their photoluminescence properties, J. Cryst. Growth 280 (2005) 99–106.
[12] S.H. Shen, L. Zhao, L.J. Guo, Morphology, structure and photocatalytic performance of $ZnIn_2S_4$ synthesized via a solvothermal/hydrothermal route in different solvents, J. Phys. Chem. Solids 69 (2008) 2426–2432.
[13] J.G. Yu, Q.J. Xiang, M.H. Zhou, Preparation, characterization and visible-light-driven photocatalytic activity of Fe-doped titania nanorods and first-principles study for electronic structures, Appl. Catal. B: Environ. 90 (2009) 595–602.
[14] X.N. Zhang, J.H. Huang, K.N. Ding, Y.D. Hou, X.C. Wang, X.Z. Fu, Photocatalytic decomposition of benzene by porous nanocrystalline $ZnGa_2O_4$ with a high surface area, Environ. Sci. Technol. 43 (2009) 5947–5951.
[15] G.S. Li, D.Q. Zhang, J.C. Yu, A new visible-light photocatalyst: CdS quantum dots embedded mesoporous TiO_2, Environ. Sci. Technol. 43 (2009) 7079–7085.
[16] J.H. Huang, X.C. Wang, Y.D. Hou, X.F. Chen, L. Wu, X.X. Wang, X.Z. Fu, Synthesis of functionalized mesoporous TiO_2 molecular sieves and their application in photocatalysis, Microporous Mesoporous Mater. 110 (2008) 543–552.
[17] Z.F. Zhu, H.J. Sun, H. Liu, D. Yang, PEG-directed hydrothermal synthesis of alumina nanorods with mesoporous structure via AACH nanorod precursors, J. Mater. Sci. 45 (2010) 46–50.
[18] H. Firouzabadi, N. Iranpoor, M. Gholinejad, One-pot thioetherification of aryl halides using thiourea and alkyl bromides catalyzed by copper(i) iodide free from foul-smelling thiols in wet polyethylene glycol (PEG 200), Adv. Synth. Catal. 352 (2010) 119–124.
[19] F. Dong, W.R. Zhao, Z.B. Wu, S. Guo, Band structure and visible light photocatalytic activity of multi-type nitrogen doped TiO_2 nanoparticles prepared by thermal decomposition, J. Hazard. Mater. 162 (2009) 763–770.
[20] C. West, R. Mokaya, Nanocasting of high surface area mesoporous Ga_2O_3 and GaN semiconductor materials, Chem. Mater. 21 (2009) 4080–4086.
[21] Y.M. Luo, Z.Y. Hou, J. Gao, D.F. Jin, X.M. Zheng, Synthesis of high crystallization beta-Ga_2O_3 micron rods with tunable morphologies and intensive blue emission via solution route, Mater. Sci. Eng. B: Solid 140 (2007) 123–127.
[22] Z.B. Wu, F. Dong, W.R. Zhao, S. Guo, Visible light induced electron transfer process over nitrogen doped TiO_2 nanocrystals prepared by oxidation of titanium nitride, J. Hazard. Mater. 157 (2008) 57–63.
[23] J.H. Mo, Y.P. Zhang, Q.J. Xu, Y.F. Zhu, J.J. Lamson, R.Y. Zhao, Determination and risk assessment of by-products resulting from photocatalytic oxidation of toluene, Appl. Catal. B: Environ. 89 (2009) 570–576.
[24] NIOSH, REL by U.S. National Institute for Occupational Safety Health, http://www.cdc.gov/niosh/, 2008.
[25] K. Maeda, K. Domen, New non-oxide photocatalysts designed for overall water splitting under visible light, J. Phys. Chem. C 111 (2007) 7851–7861.
[26] Y. Nosaka, S. Komori, K. Yawata, T. Hirakawa, A.Y. Nosaka, Photocatalytic OH radical formation in TiO_2 aqueous suspension studied by several detection methods, Phys. Chem. Chem. Phys. 5 (2003) 4731–4735.
[27] H.B. Fu, S.C. Zhang, T.G. Xu, Y.F. Zhu, J.M. Chen, Photocatalytic degradation of RhB by fluorinated Bi_2WO_6 and distributions of the intermediate products, Environ. Sci. Technol. 42 (2008) 2085–2091.
[28] S. Tojo, T. Tachikawa, M. Fujitsuka, T. Majima, Iodine-doped TiO_2 photocatalysts: correlation between band structure and mechanism, J. Phys. Chem. C 112 (2008) 14948–14954.
[29] K. Shimamura, E.G. Villora, T. Ujiie, K. Aoki, Excitation and photoluminescence of pure and Si-doped beta-Ga_2O_3 single crystals, Appl. Phys. Lett. 92 (2008) 201914.
[30] S.C. Yan, L.J. Wan, Z.S. Li, Y. Zhou, Z.G. Zou, Synthesis of a mesoporous single crystal Ga_2O_3 nanoplate with improved photoluminescence and high sensitivity in detecting CO, Chem. Commun. 46 (2010) 6388–6390.
[31] H.Q. Yang, R.Y. Shi, J. Yu, R.N. Liu, R.G. Zhang, H. Zhao, L.H. Zhang, H.R. Zheng, Single-crystalline beta-Ga_2O_3 hexagonal nanodisks: synthesis, growth mechanism, and photocatalytic activities, J. Phys. Chem. C 113 (2009) 21548–21554.
[32] A. Khan, W.M. Jadwisienczak, M.E. Kordesch, One-step preparation of ultra-wide beta-Ga_2O_3 microbelts and their photoluminescence study, Physica E 35 (2006) 207–211.

[33] K.Y. Jung, S.B. Park, M. Anpo, Photoluminescence and photoactivity of titania particles prepared by the sol–gel technique: effect of calcination temperature, J. Photochem. Photobiol. A 170 (2005) 247–252.
[34] Y. Li, X.Y. Yang, J. Rooke, G. van Tendeloo, B.L. Su, Ultralong $Cu(OH)_2$ and CuO nanowire bundles: PEG200-directed crystal growth for enhanced photocatalytic performance, J. Colloid Interface Sci. 348 (2010) 303–312.
[35] X.X. Shi, L.L. Pan, S.P. Chen, Y. Xiao, Q.Y. Liu, L.J. Yuan, J.T. Sun, L.T. Cai, Zn(II)-PEG 300 globules as soft template for the synthesis of hexagonal ZnO micronuts by the hydrothermal reaction method, Langmuir 25 (2009) 5940–5948.